RSC Advances

PAPER

View Article Online
View Journal | View Issue

Cite this: *RSC Adv.*, 2015, **5**, 20178

Carbon concentration dependent grain growth of Cu_2ZnSnS_4 thin films

Vincent Tiing Tiong,[a] Yi Zhang,[b] John Bell[a] and Hongxia Wang*[a]

Organic solvents are commonly used in ink precursors of Cu_2ZnSnS_4 (CZTS) nanocrystals to make thin films for applications such as solar cells. However, the traces of carbon residual left behind by the organic solvents after high-temperature annealing is generally considered to restrict the growth of nanocrystals to form large grains. This work reported the first systematic study on the influence of carbon content of organic solvents on the grain growth of CZTS nanomaterial during high temperature sulfurization annealing. Solvents with carbon atom per molecule varying from 3 to 10 were used to made ink of CZTS nanocrystals for thin film deposition. It has been found that, after high temperature sulfurization annealing, a bilayer structure was formed in the CZTS film using organic solvent containing 3 carbon atoms per solvent molecule based on glycerol and 1,3-propanediol. The top layer consisted of closely-packed large grains and the bottom layer was made of as-synthesized nanoparticles. In contrast, the CZTS film made with the solvent molecule with more carbon atoms including 1,5-pentanediol (5 carbon atoms) and 1,7-heptanediol (7 carbon atoms) consisted of nanoparticles embedded with large crystals. It is believed that the carbon residues left behind by the organic solvents affected the necking of CZTS nanocrystals to form large grains through influencing the surface property of nanocrystals. Furthermore, it has also been observed that the solvent affected the thickness of MoS_2 layer which was formed between CZTS and Mo substrate. A thinner MoS_2 film (50 nm) was obtained with the slurry using carbon-rich terpineol as solvent whereas the thickest MoS_2 (350 nm) was obtained with the film made from 1,3-propanediol based solvent. The evaluation of the photoactivity of the CZTS thin films has demonstrated that a higher photocurrent was generated with the film containing more large grains.

Received 16th December 2014
Accepted 11th February 2015

DOI: 10.1039/c4ra16447d

www.rsc.org/advances

1. Introduction

Cu_2ZnSnS_4 (CZTS) has received substantial attention as a material for next generation thin film solar cells due to its promise for delivering cost-effective solar electricity. Solely consisting of non-toxic, earth abundant and inexpensive elements, CZTS offers high absorption coefficient of $\sim 10^4$ cm^{-1} with an optimum direct bandgap of 1.5 eV.[1–4] CZTS thin films can be produced by conventional vacuum-based technologies, such as sputtering and evaporation, which have proven their capability in producing high efficiency solar cells such as Cu(In,Ge)Se_2 (CIGS).[5] However, these technologies normally undergo relatively high energy consumption and have low growth rates which make them neither cheap nor viable for large-scale production. Alternatively, non-vacuum, low-temperature solution-based approaches are considered more cost-effective for large scale production of CZTS thin films for solar cells. Up-to-now, the CZTSSe device with a record efficiency of 12.6% was made by a hydrazine-based solution process, which demonstrates the potential of solution-method for producing low cost, high performance PV devices.[6–8]

The process of solution-based thin film deposition normally involves dispersion of CZTS nanocrystals or nanocrystal precursor in a suitable organic solvent or solvent mixture to form an ink precursor for film deposition. Generally speaking, the role of the solvent is to improve the dispersion and homogeneity of the ink, which will be helpful to increase the quality of subsequently deposited film. Nevertheless, the solvent needs to be removed to ensure a good electrical contact of the nanocrystals before the film can be used in devices. A high temperature annealing is normally used for this purpose. In addition, high temperature annealing also serves as a way to induce grain growth of the nanocrystals in the deposited films[9] because large grains is known to benefit the performance of solar cells through reduced grain boundaries.[10]

Most organic solvents used in the ink precursor of CZTS nanocrystals contain carbon atoms. Although the solvents are expected to be burn out at high temperature annealing, however, carbon residual trace left behind by the organic solvents has been reported, which may influence the grain growth of nanocrystals at high temperature.[11] Our previous

[a]*School of Chemistry, Physics and Mechanical Engineering, Science and Engineering Faculty, Queensland University of Technology, Brisbane, QLD 4001, Australia. E-mail: hx.wang@qut.edu.au*

[b]*Institute of Photoelectronic Thin Film Devices and Technology, Nankai University, Tianjin 300071, China*

research has shown that CZTS nanocrystals annealed at 550 °C for 30 min remained in nanometre sizes when terpineol and Triton X-100 which are rich in carbon were used in the ink precursor.[9] In contrast, CZTS nanocrystals could grow to several hundred nanometres when ethylene glycol which has only two carbon atoms in its molecule was used in the film formation process.[12] These results suggest that the growth of CZTS nanocrystals strongly depends on the solvent used in the ink of nanocrystals for film deposition.

The present work investigated the influence of solvent used in the ink precursor of CZTS nanocrystals on the subsequent grain growth of CZTS in thin films. The solvent studied contains different number (3–10) of carbon atom per molecule. It has been found that a layer of large grains was formed on the surface of the deposited CZTS film made with the solvent based on glycerol and 1,3-propanediol which contain only three carbon atoms per molecule. In contrast, the film consisting of small grains embedded with randomly distributed large grains was obtained when carbon-rich solvent such as 1,5-pentanediol or 1,7-heptanediol was used in the ink. Moreover, the influence of the organic solvents on the formation of MoS_2 layer in the film was also investigated. The photoactivity of the annealed CZTS films was evaluated and the results have shown that the film with more large grains generated a higher photocurrent density under illumination.

2. Experiments

2.1. Synthesis of CZTS nanocrystals

All the chemicals used in this work were provided by Sigma Aldrich and used as received unless otherwise stated. The synthesis of CZTS nanocrystals were reported previously by us.[13] Briefly, in a typical experimental procedure, analytical grade of copper(II) chloride dehydrate ($CuCl_2 \cdot 2H_2O$, 0.2 mmol), zinc chloride ($ZnCl_2$, 0.12 mmol, product of BDH), tin(IV) chloride pentahydrate ($SnCl_4 \cdot 5H_2O$, 0.11 mmol), sodium sulphide nonahydrate ($Na_2S \cdot 9H_2O$, 0.5 mmol) and thioglycolic acid (TGA, 18 μL) were dissolved in 34 mL Milli-Q water under vigorous magnetic stirring. The solution was then transferred to a Teflon-lined stainless steel autoclave (Parr Instrument Company) of 45 mL capacity which was then sealed and maintained at 240 °C for 24 h. After that, the autoclave was allowed to cool to room temperature naturally. The black precipitate was collected by centrifugation and washed with deionised water and absolute ethanol for several times to remove the ions in the end product. Finally, the hydrothermal product of CZTS nanocrystals was vacuum-dried at 60 °C for 5 h. The as-synthesized material was pure CZTS with kesterite structure and did not contain secondary phases according to our previous study.[13]

2.2. Deposition of CZTS thin films

A series of ink solution were prepared by dispersing the as-synthesised CZTS nanocrystals (15%, w/w) in different solvent including glycerol, 1,3-propanediol, 1,5-pentanediol, or 1,7-heptanediol (Alfa Aesar). For comparison, the standard ink solution that contained CZTS (10%, w/w) in a mixture of terpineol and Triton X-100 (85% : 5%, w/w) was also prepared according to our previous work.[9] All the slurries were subject to rigorous magnetic stirring for 48 hours at 60 °C. A thin film was made by depositing the CZTS ink on Mo/soda lime glass (SLG) substrate by doctor-blading method. The substrate was pre-washed thoroughly with deionised water, acetone, and ethanol in sequence under sonication for 10 min followed by blow-dried with nitrogen gas. The nanocrystal films were then pre-annealed on a hot plate at 300 °C for 10 min in air before being placed in a graphite box containing sulfur powder and annealed at 600 °C for 1 h by a rapid thermal processing (RTP) system with a heating rate of 50 °C min^{-1}. A constant annealing atmosphere of 0.3 atm argon gas was supplied in the RTP furnace.

For clarity, the CZTS film prepared using solvent (i) glycerol is named as CZTS-G-3C; (ii) 1,3-propanediol is named as CZTS-P-3C; (iii) 1,5-pentanediol is named as CZTS-N-5C; (iv) 1,7-heptanediol is named as CZTS-H-7C; and (v) the solvent mixture of terpineol and Triton X-100 is named as CZTS-T in the following context. The digit number indicates the number of carbon atom per solvent molecule.

2.3. Characterisation

The crystallographic structure of the synthesized samples was identified by a multi-purpose X-ray diffractometer (XRD, PAN-analytical XPert Pro, Cu Kα, $\lambda = 0.154056$ nm). A Raman spectrometer (Renishaw inVia Raman microscope) with a laser excitation wavelength of 785 nm was used to record the Raman spectrum of the material at room temperature. The Raman spectrum was collected by taking the average of 10 different spots. The morphology and composition of the samples were characterized by a field emission scanning electron microscope (FESEM, JEOL 7001F) at an acceleration voltage of 20.0 kV combined with an energy dispersive X-ray spectroscopy (EDS). The photoresponse of the CZTS thin films was evaluated by a three-electrode photoelectrochemical (PEC) cell which consisted of CZTS/Mo/SLG based working electrode, platinum wire counter electrode and Ag/AgCl reference electrodes in an aqueous electrolyte solution containing 0.2 M $Eu(NO_3)_3$ (pH = 2.2). The CZTS electrode was illuminated by a light emitting diode (LED, 532 nm) with light intensity of 50 mW cm^{-2}. The photocurrent generated by the PEC cell was recorded by an electrochemical workstation (VSP BioLogic) under a constant potential of −300 mV (*vs.* saturated Ag/AgCl reference electrode).

3. Results and discussion

Fig. 1(a) and (b) illustrate the cross-sectional and top-view SEM images of a typical film consisting of as-synthesized CZTS nanocrystals prior to thermal treatment. The film consists of nanoparticles with size around 50–60 nm and has a uniform film thickness around 3.0 μm. Large cracks can be seen in the surface of the film after solvent is dried out. Fig. 1(c) illustrates the SEM cross-sectional image of the annealed CZTS-G-3C film using glycerol as solvent in the ink precursor. Compared to the

film shown in Fig. 1(a) and (b), a distinct feature of bi-layer structure is clearly seen with CZTS-G-3C. The top layer consists of large grains with thickness around 0.5 μm and the bottom layer is made of fine grains with thickness around 2.8 μm. As shown in Fig. 1(d), the crystal size in the top layer is up to 3.0 μm and the grains are closely connected with each other to form a compact layer although small holes are found in some area of the film. In contrast, the size of nanoparticles in the bottom layer is very similar to that of the as-synthesized CZTS nanocrystals. This suggests that grain growth mainly occurred on the surface of the film. Similar to glycerol, a bi-layer structure is also observed with CZTS-P-3C film shown in Fig. 1(e). The average thickness of the top layer of large crystals is around 0.8 μm and the bottom layer composed of small nanocrystals has a thickness of 1.7 μm. Compared to CZTS-G-3C where the height of the large grains in the top layer is very uniform, the height of the crystals in the top layer of CZTS-P-3C film varies significantly. Meanwhile, the surface image shown in Fig. 1(f) indicates that the top layer of the CZTS-P-3C film is composed of much smaller grains (hundreds of nanometres) compared to that of CZTS-G-3C film illustrated in Fig. 1(d). Another feature of the CZTS-P-3C film is that the surface of the film is more compact and no holes are observed.

In contrast, when 1,5-pentanediol and 1,7-heptanediol were used in the ink precursors (Fig. 1(g)–(j)), the separation between the fine-grained layer and large-grained layer in the films is not as distinguishable as that in CZTS-G-3C and CZTS-P-3C films. The CZTS-N-5C film (Fig. 1(g)) consists of 1.7 μm fine-grained layer with large crystals with size up to 1 μm embedded in the nanoparticles. The top-view image of the film shown in Fig. 1(h) demonstrates the CZTS-N-5C film is porous and consists of a mixture of nanocrystals and randomly distributed large crystals. Similar phenomenon is also observed in CZTS-H-7C film but with more pores and cracks (Fig. 1(i) and (j)). Compared to the CZTS-N-5C film, clearly the surface of the CZTS-H-7C film has a less coverage of large crystals. Fig. 1(k) and (l) displays the SEM images of the standard film using the mixture of carbon rich materials of terpineol and Triton X-100 in the nanocrystal ink where terpineol contains 10 carbon atoms per molecule and Triton X-100 contains 14 carbon atoms per molecule. As can be seen, the main body of the film consists of as-synthesized CZTS nanoparticles. Some large crystals which are randomly distributed on the film surface can also be seen. The cross-sectional SEM in Fig. 1(k) indicates that the there is no large crystals in the bulk of the film. Clearly, CZTS-T film has the least content of large crystals among the films investigated.

The above results clearly demonstrate the effect of organic solvents in the ink precursor on the subsequent grain growth of CZTS nanocrystals in thin films during annealing. Generally, the more carbon atoms the solvent molecule has, the less content of large grains is formed in the CZTS thin film. Glycerol and 1,3-propanediol which contains only three carbon atoms in their molecule have shown the most significant grain growth in the film. When the carbon content of the solvent molecule is increased to 5 and 7 as in the case of 1,5-pentanediol and 1,7-heptanediol, the grain growth is significantly restricted as demonstrated by the reduced coverage of large crystals in the film surface and the reduction in the average crystal sizes. By further increasing the carbon atoms in the solvent molecule to 10 (CZTS-T), the content of large crystals was further reduced.

It is known that small crystals have the tendency to grow to large ones under high temperature annealing according to Ostwald ripening mechanism, a process which is thermodynamically driven by the high surface energy of small crystals. The surface energy of small crystals decreases and becomes more stable by growing to large crystals. The SEM images in Fig. 1 indicate that the grain growth mainly occurs on the surface of the deposited thin films in the case of CZTS-G-3C, CZTS-P-3C and CZTS-T. However, the porous film of CZTS-N-5C and CZTS-H-7C contain large crystals across the whole

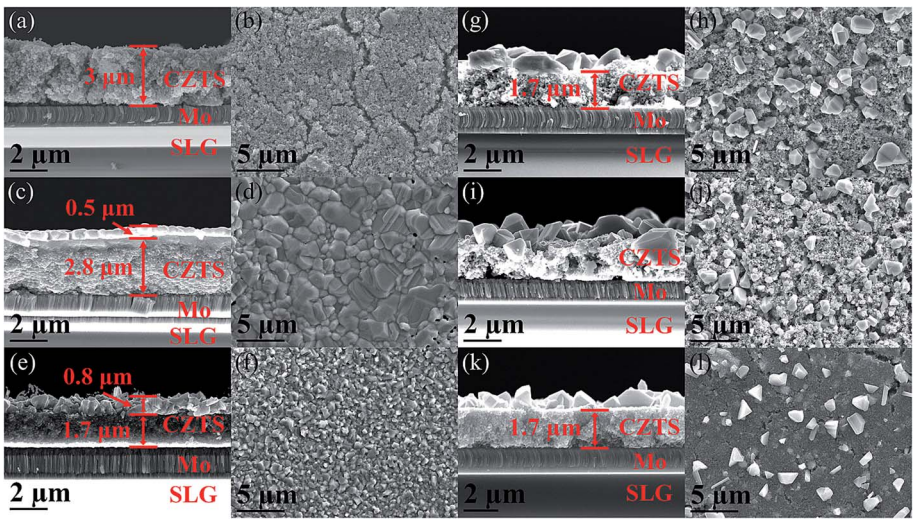

Fig. 1 Cross-sectional and top-view SEM images of a typical film of as-synthesized CZTS nanocrystals (a and b), and the annealed film made from CZTS nanocrystals ink in solvent based on CZTS-G-3C (c and d), CZTS-P-3C (e and f), CZTS-N-5C (g and h), CZTS-H-7C (i and j), and CZTS-T (k and l) at 600 °C for 1 h.

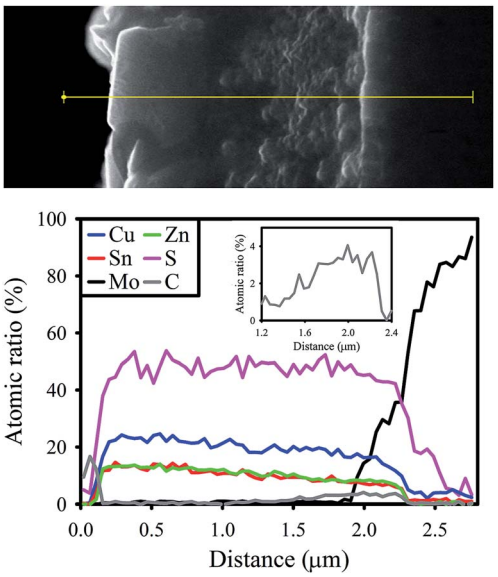

Fig. 2 The SEM image and the corresponding EDS line scan along the yellow line of the CZTS-G-3C film (inset figure shows the enlarged plot of EDS line scan of carbon).

film. In order to understand this phenomenon, the chemical composition between the large crystals and small crystals was studied by energy-dispersive X-ray spectroscopy (EDS). The EDS line scan showing the distribution of Cu, Zn, Sn, S and carbon in CZTS-G-3C which has a distinctive bilayer structure of large grains and small crystals is illustrated in Fig. 2. The results show that the distribution of Cu, Sn, Zn, S is generally uniform across the whole film. However, a slight increase of the content of carbon which is nearly zero in the top layer of large grains is found in the bottom layer of nanocrystals as shown in the inset of Fig. 2. This result not only confirms the existence of carbon residue traces left behind by the organic solvent used in the ink precursor, but also indicates the impact of carbon traces on the grain growth of nanocrystals in the film. That is, in order for the growth of nanocrystals to occur, the carbon residues need to be removed first.

The nanocrystals were surrounded by the organic solvent used in the ink. Under high temperature annealing, the solvent was evaporated and then removed through interaction with sulfur vapour to form COS or CS_2 and H_2S.[14] The solvent which was not removed completely will leave carbon residuals on the surface of the as-synthesized nanocrystals to form a coating layer. Such a coating layer probably affects the surface property of the nanocrystals including reducing the surface energy of the crystals or may create energy barrier for the growth of nanocrystals, which hinders the growth of nanocrystals. Thus, in order for the grain growth to occur, the surface of the nanocrystals needs to be cleaned firstly.

As shown by the SEM images in Fig. 1, large grains were mainly formed on the top layer of the CZTS film. This is probably due to the fact that the nanoparticles on the film surface were well exposed to sulfur vapour during high temperature annealing, allowing a relatively complete reaction between sulfur and the carbon containing solvent on the surface of the CZTS nanoparticles. However, such reaction is probably less efficient for the nanoparticles in the bulk of the film because of the increased physical barrier for diffusion of sulfur to the film. The sulfur vapour has to diffuse through the nanoparticles on the surface of the film first before reaching the nanoparticles underneath. As a result, the amount of sulfur vapour available for the reaction with carbon in the bulk of the film should be less compared to the sulfur content on the film surface. In addition, the clear bilayer structure in the film based on CZTS-G-3C and CZTS-P-3C suggests that the nanoparticles that are surface-cleaned by sulfur vapour grow to large crystals and the necking of large grains leads to the formation of the top layer in the film. The compact top layer of large grains may further hinder the transport pathway of sulfur vapour to the nanoparticles underneath, resulting in carbon residues trapped in the bottom layer as confirmed by the EDS results in Fig. 2. As a consequence, the nanocrystals in the bulk of the film cannot grow to large ones.

If the above hypothesis is correct, a thicker layer of carbon residues is expected for the solvent with more carbon content compared to the solvent with less carbon content. Hence, more sulfur is needed to interact with these carbon residues to form a clean surface of CZTS nanocrystals for crystal growth. Under the condition of a constant sulfur vapour pressure as used in this work, it is reasonable to speculate that the crystal growth rate is slower in the films using carbon-rich solvent such as CZTS-N-5C and CZTS-H-7C as well as CZTS-T compared to the less carbon based CZTS-G-3C and CZTS-P-3C. The much less amount of large crystals in the carbon-rich solvent based film as seen in the SEM images in Fig. 1 suggests that the sulfur vapour pressure used in this work might not be sufficient to remove the carbon residuals on the surface of these film. A scheme describing the impact of carbon residues on the grain growth of CZTS thin film is illustrated in Fig. 3.

Furthermore, it is found that the solvent used in the ink precursor for film deposition also affected the thickness of MoS_2 layer which was formed on the Mo electrical substrate. Previous reports by Scragg *et al.* have shown that a layer of MoS_2 formed in CZTS film is detrimental for the performance of solar cells, in particularly the short circuit current of the device.[15,16] Fig. 4 shows the enlarged cross-sectional SEM images of the annealed films made with the nanocrystal inks containing different solvents. A layer of MoS_2 can be clearly seen with all the films but the thickness of the MoS_2 layer varies significantly. The MoS_2 layer in the carbon-rich CZTS-T film is around 50 nm (Fig. 4(e)) whereas the MoS_2 layer in the film made with other solvents with less carbon atoms is over 100 nm. The most significant formation of MoS_2 layer (350 nm) was obtained with CZTS-P-3C film as shown in Fig. 4(b). It is worth to note that MoS_2 layer was only observed with the Mo substrate which was interfaced with CZTS film and no MoS_2 was detected by SEM with a bare Mo film which was annealed under the same sulfurization condition. However, Scragg *et al.* has reported that the formed MoS_2 layer on a bare Mo substrate is no more than 5 nm which cannot be seen by SEM but could be detected by Raman spectroscopy.[17] Nevertheless, such thickness is negligible compared to the MoS_2 layer formed in the CZTS film in

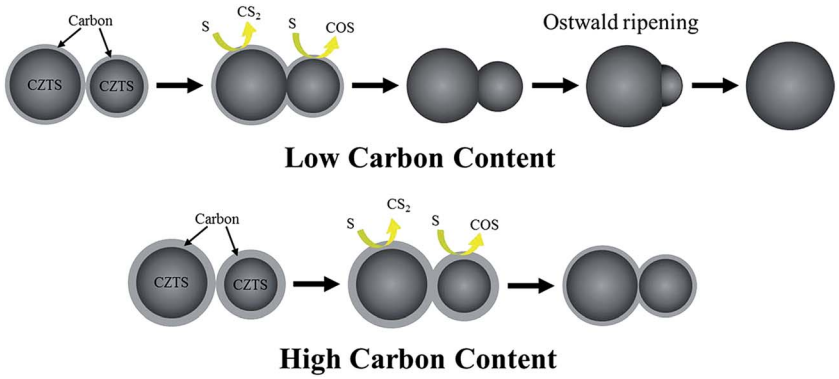

Fig. 3 Schematic illustration of the impact of coating of carbon residues on the grain growth of CZTS nanoparticles during sulfurization annealing.

this work. It is therefore rational to speculate that the MoS_2 layer was formed through reaction of Mo with CZTS rather than with sulfur vapour. According to Scragg *et al.*, the chemical reaction between Mo and CZTS is thermodynamically favoured and Mo is oxidized while SnS_2 is reduced,[17] leading to the reaction products of Cu_2S, ZnS, SnS and MoS_2. However, the largely unchanged distribution of S content shown in Fig. 2 and Table 1 below suggests that the sulfur loss in CZTS was later compensated in time by the high temperature sulfur vapour. The different thickness of the MoS_2 layer suggests that the solvent used in the ink might also influence aforementioned chemical reactions between CZTS and Mo.

The chemical compositions of the as-synthesised CZTS nanocrystals and the annealed CZTS films prepared with different slurry solvents are shown in Table 1. The atomic ratios of [Cu]/([Zn] + [Sn]) and [Zn]/[Sn] of the as-synthesised CZTS nanocrystals are 0.88/1 and 1.07/1, respectively. After sulfurization annealing, the Cu content is largely unchanged by considering the experimental errors of EDS. However, a decrease of Zn content was found with all the samples except for CZTS-P-3C, leading to all the films with composition of Cu-poor and Sn-rich. The content of sulfur in all the sulphurised films increased slightly compared to the as-synthesized CZTS nanocrystals, confirming the diffusion of sulphur vapour into the film of CZTS nanocrystals during the annealing process. Compared to other films, the chemical composition of CZTS-P-3C film is nearly identical with the as-synthesized CZTS nanocrystals. Considering this film also shows the most significant growth of MoS_2, we suspects the organic solvent in the CZTS nanocrystal ink might involve in the interaction between Mo and CZTS and the loss of Zn. But the exact reaction mechanism is still unclear at this stage.

In order to clarify whether the loss of Zn at high temperature annealing could cause any changes in the crystal structure of the material, the XRD patterns and Raman spectra of the annealed CZTS films deposited with different solvents were investigated. As shown in Fig. 5(a), all the XRD peaks of the annealed CZTS films can be indexed to the corresponding crystallographic planes of kesterite CZTS (JCPDS 01-75-4122) and no peak corresponding to secondary phase was detected. Although the SEM images of all the films show the formation of MoS_2 at the back contact, MoS_2 (JCPDS 24-0513) was only detected in the CZTS-P-3C film. This is probably due to the thicker MoS_2 formed in the CZTS-P-3C film as compared to other films. Since metal sulfides such as ZnS and Cu_2SnS_3 have similar XRD patterns with CZTS due to their similarity in the crystal structure, it is vital to employ Raman spectroscopy to confirm the phase purity of the annealed CZTS films. The Raman spectra illustrated in Fig. 5(b) shows that all the Raman peaks of the annealed films at 265, 287, 338, 367 and 375 cm^{-1} can be assigned to the Raman scattering of kesterite CZTS.[7] The

Table 1 Elemental composition of the annealed CZTS films prepared with different solvent in nanocrystal ink precursor

Samples	Cu (%)	Zn (%)	Sn (%)	S (%)	[Cu]/([Zn] + [Sn])	[Zn]/[Sn]
CZTS	24.18	14.27	13.30	48.25	0.88/1	1.07/1
CZTS-G-3C	23.46	12.93	13.01	50.60	0.90/1	0.99/1
CZTS-P-3C	22.27	12.72	12.57	52.44	0.88/1	1.01/1
CZTS-N-5C	23.89	12.46	13.03	50.62	0.94/1	0.95/1
CZTS-H-7C	22.86	11.22	13.80	52.12	0.91/1	0.81/1
CZTS-T	22.46	11.33	13.86	52.35	0.89/1	0.82/1

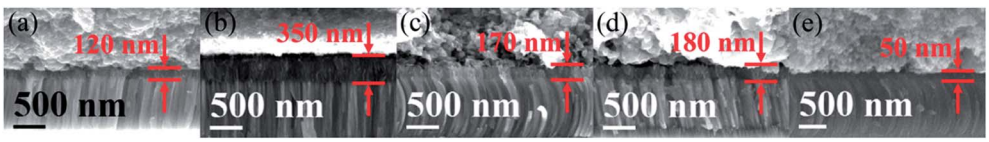

Fig. 4 Comparison of the MoS_2 layer formed between CZTS and Mo substrate in the films based on CZTS-G-3C (a), CZTS-P-3C (b), CZTS-N-5C (c), CZTS-H-7C (d), and CZTS-T (e). All the films were annealed at 600 °C for 1 h.

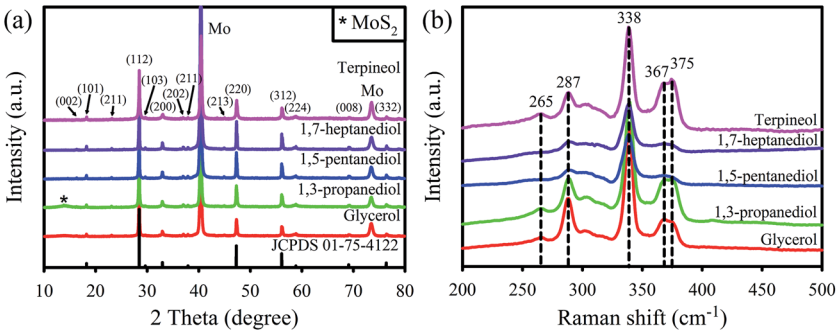

Fig. 5 (a) XRD patterns and (b) Raman spectra of the annealed CZTS films prepared with different slurry formulations.

Raman peaks of CZTS-N-5C and CZTS-H-7C films are weaker and broader compared to other films. This could be due to the variation in the crystallite size, in particular the nanometer sized crystals.[19,20] The characteristic Raman peaks of possible secondary phases due to decomposition of CZTS such as $Cu_{2-x}S$ (475 cm^{-1}), SnS_2 (315 cm^{-1}), ZnS (278 and 351 cm^{-1}), Cu_2SnS_3 (297 and 337 cm^{-1}) and Cu_3SnS_4 (318 cm^{-1}) were not found in Fig. 5(b).[19,21] Therefore, we conclude that the Zn loss in the film was too small to cause structure change of the CZTS materials. Another general issue on CZTS is the loss of Sn which is commonly found in CZTS material at high temperature annealing (above 500 °C) owing to the relatively high vapour pressure of tin sulfides.[17,18] The absence of Sn-loss in the annealed film in our work suggests the decomposition of CZTS was effectively hindered in the presence of sulfur vapour during the thermal annealing process.[22]

The photoactivity of the prepared CZTS thin films was evaluated using a three-electrode configuration cell setup under illumination of a single wavelength provided by a light emitting diode (532 nm) and the results are shown in Fig. 6. Apparently, all the samples generated photocurrent under the illumination. However, the largest photocurrent density gain of 0.43 mA cm^{-2} was obtained with CZTS-G-3C film among the films investigated (Fig. 6(a)). Moreover, a dramatic decay of the photocurrent was observed with the film under continuous illumination. This could be due to the electron–hole recombination at the CZTS grain boundaries. Under the same condition, the CZTS-P-3C film generated a photocurrent density of 0.38 mA cm^{-2} with less photocurrent decay (Fig. 6(b)). Compared to CZTS-P-3C film, CZTS-N-5C generated a further lower photocurrent density with J_{sc} = 0.32 mA cm^{-2} (Fig. 6(c)). The lowest J_{sc} was produced by CZTS-H-7C film which has a J_{sc} = 0.15 mA cm^{-2} under the same illumination condition (Fig. 6(d)). This tremendous drop in J_{sc} is attributed to the poor electrical contact between the grains in the film which had more cracks and pores. By comparing the generated photocurrent density of CZTS-G-3C and CZTS-P-3C films both of which have bilayer structure, it seems that the large-grained layer in the film is most likely to be responsible for the observed photocurrent of the films. Surprisingly, nearly 0.23 mA cm^{-2} of photocurrent density was generated by CZTS-T film even though the content of large-crystals in the film was the lowest among the film investigated (Fig. 6(e)). The results suggest that besides grain sizes, the homogeneity of the film also affects photoactivity of the CZTS light absorber material.

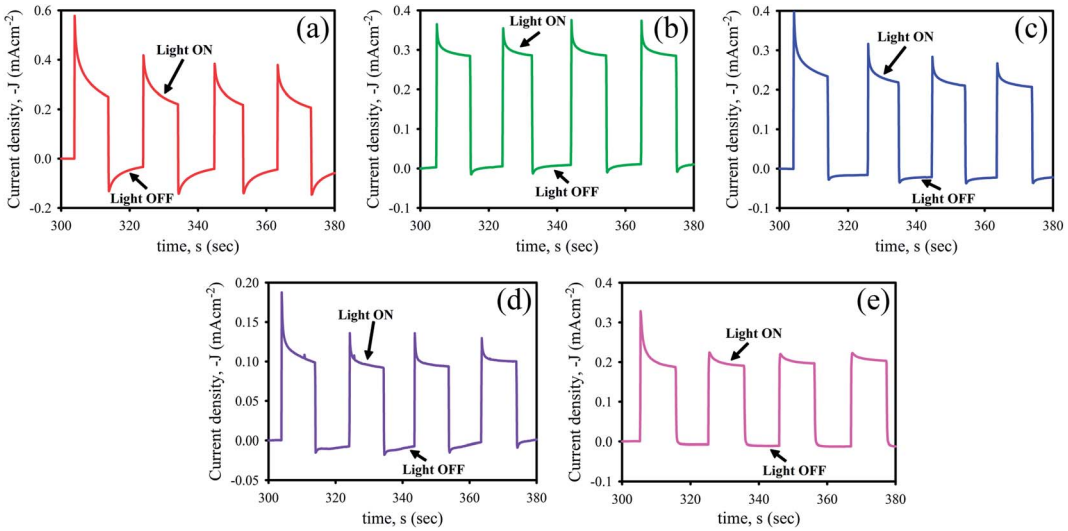

Fig. 6 Photoresponse of the CZTS films based on (a) CZTZ-G-3C, (b) CZTS-P-3C, (c) CZTS-N-5C, (d) CZTS-H-7C, and (e) CZTS-T.

4. Conclusion

The impact of the content of carbon atom in the solvent used in the ink precursor of CZTS nanocrystals on the subsequent grain growth of CZTS film during sulfurization annealing was investigated. It has been found that the carbon residual left by the organic solvent significantly restricted the growth of nanocrystals to form large grains. A layer of large crystals were found on the surface of the CZTS film using glycerol and 1,3-propanediol as solvent which contains only three carbon atoms in their molecule. In contrast, the coverage of large crystals in the film was reduced using solvents with a higher content of carbon atom per molecule such as 1,5-pentanediol, 1,7-heptanediol and terpineol. Moreover, it has also been found that the solvent affected the thickness of MoS_2 layer which was formed on the Mo substrate. It is speculated that the carbon residual left behind by the organic solvent makes the grain growth thermodynamically unfavourable. In addition, the formation of large grains on the surface of the film suggests that the carbon residues can be removed through sulfurization. The compositional analysis has revealed that the high temperature sulfurization did not cause phase decomposition of CZTS compound although Zn-loss was found with some of the films. The investigation of the photoactivity of the film has shown that the CZTS-G-3C film generated the highest photocurrent density which is attributed to the formation of larger crystals on the surface of deposited CZTS layer. A trend of reduction in the photoactivity was observed with the increase of the carbon content per solvent molecule. Nonetheless, the homogeneity and electrical contact of the particles in the film is very crucial for generation of higher photocurrent as well.

Acknowledgements

This work was funded by Australian Research Council (ARC) Future Fellowship (FT120100674), Australia. Yi Zhang acknowledges the financial support from National Natural Science Foundation of China (61274053). The authors appreciate the technical support for material characterization by Institute of Future Environment, Queensland University of Technology.

References

1 H. Katagiri, Cu_2ZnSnS_4 thin film solar cells, *Thin Solid Films*, 2005, **480–481**, 426–432.
2 H. Wang, Progress in Thin Film Solar Cells Based on Cu_2ZnSnS_4, *Int. J. Photoenergy*, 2011, 801292.
3 J. J. Scragg, P. J. Dale, L. M. Peter, G. Zoppi and I. Forbes, New routes to sustainable photovoltaics: evaluation of Cu_2ZnSnS_4 as an alternative absorber material, *Phys. Status Solidi B*, 2008, **245**, 1772–1778.
4 S. C. Riha, B. A. Parkinson and A. L. Prieto, Solution-Based Synthesis and Characterization of Cu_2ZnSnS_4 Nanocrystals, *J. Am. Chem. Soc.*, 2009, **131**, 12054–12055.
5 P. Jackson, D. Hariskos, E. Lotter, S. Paetel, R. Wuerz, R. Menner, W. Wischmann and M. Powalla, New world record efficiency for Cu(In,Ga)Se_2 thin-film solar cells beyond 20%, *Prog. Photovoltaics*, 2011, **19**, 894–897.
6 M. T. Winkler, W. Wang, O. Gunawan, H. J. Hovel, T. K. Todorov and D. B. Mitzi, Optical designs that improve the efficiency of $Cu_2ZnSn(S,Se)_4$ solar cells, *Energy Environ. Sci.*, 2014, **7**, 1029–1036.
7 H. Katagiri, K. Jimbo, S. Yamada, T. Kamimura, W. S. Maw, T. Fukano, T. Ito and T. Motohiro, Enhanced Conversion Efficiencies of Cu_2ZnSnS_4-Based Thin Film Solar Cells by Using Preferential Etching Technique, *Appl. Phys. Express*, 2008, **1**, 2.
8 B. Shin, O. Gunawan, Y. Zhu, N. A. Bojarczuk, S. J. Chey and S. Guha, Thin film solar cell with 8.4% power conversion efficiency using an earth-abundant Cu_2ZnSnS_4 absorber, *Prog. Photovoltaics*, 2013, **21**, 72–76.
9 V. T. Tiong, Y. Zhang, J. Bell and H. Wang, Phase-selective hydrothermal synthesis of Cu_2ZnSnS_4 nanocrystals: the effect of the sulphur precursor, *CrystEngComm*, 2014, **16**, 4306–4313.
10 C. Steinhagen, M. G. Panthani, V. Akhavan, B. Goodfellow, B. Koo and B. A. Korgel, Synthesis of Cu_2ZnSnS_4 Nanocrystals for Use in Low-Cost Photovoltaics, *J. Am. Chem. Soc.*, 2009, **131**, 12554–12555.
11 À. Carreté, A. Shavel, X. Fontané, J. Montserrat, J. Fan, M. Ibáñez, E. Saucedo, A. Pérez-Rodríguez and A. Cabot, Antimony-Based Ligand Exchange to Promote Crystallization in Spray-Deposited $Cu_2ZnSnSe_4$ solar cells, *J. Am. Chem. Soc.*, 2013, **135**, 15982–15985.
12 Q. Tian, X. Xu, L. Han, M. Tang, R. Zou, Z. Chen, M. Yu, J. Yang and J. Hu, Hydrophilic Cu_2ZnSnS_4 nanocrystals for printing flexible, low-cost and environmentally friendly solar cells, *CrystEngComm*, 2012, **14**, 3847–3850.
13 V. T. Tiong, J. Bell and H. Wang, One-step synthesis of high quality kesterite Cu_2ZnSnS_4 nanocrystals – a hydrothermal approach, *Beilstein J. Nanotechnol.*, 2014, **5**, 438–446.
14 B. D. Chernomordik, A. E. Beland, D. D. Deng, L. F. Francis and E. S. Aydil, Microstructure Evolution and Crystal Growth in Cu_2ZnSnS_4 Thin Films Formed By Annealing Colloidal Nanocrystal Coatings, *Chem. Mater.*, 2014, **26**, 3191–3201.
15 J. Li, Y. Zhang, H. Wang, L. Wu, J. Wang, W. Liu, Z. Zhou, Q. He and Y. Sun, On the growth process of $Cu_2ZnSn(S,Se)_4$ absorber layer formed by selenizing Cu–ZnS–SnS precursors and its photovoltaic performance, *Sol. Energy Mater. Sol. Cells*, 2015, **132**, 363–371.
16 J. J. Scragg, T. Kubart, J. T. Watjen, T. Ericson, M. K. Linnarsson and C. Platzer-Bjorkman, Effects of Back Contact Instability on Cu_2ZnSnS_4 Devices and Processes, *Chem. Mater.*, 2013, **25**, 3162–3171.
17 J. J. Scragg, J. T. Wätjen, M. Edoff, T. Ericson, T. Kubart and C. Platzer-Björkman, A Detrimental Reaction at the Molybdenum Back Contact in $Cu_2ZnSn(S,Se)_4$ Thin-Film Solar Cells, *J. Am. Chem. Soc.*, 2012, **134**, 19330–19333.
18 A. Redinger, D. M. Berg, P. J. Dale and S. Siebentritt, The Consequences of Kesterite Equilibria for Efficient Solar Cells, *J. Am. Chem. Soc.*, 2011, **133**, 3320–3323.
19 A. J. Cheng, M. Manno, A. Khare, C. Leighton, S. A. Campbell and E. S. Aydil, Imaging and phase identification of

Cu_2ZnSnS_4 thin films using confocal Raman spectroscopy, *J. Vac. Sci. Technol., A*, 2011, **29**, 051203–051211.

20 P. M. P. Salomé, J. Malaquias, P. A. Fernandes, M. S. Ferreira, A. F. da Cunha, J. P. Leitão, J. C. González and F. M. Matinaga, Growth and characterization of $Cu_2ZnSn(S,Se)_4$ thin films for solar cells, *Sol. Energy Mater. Sol. Cells*, 2012, **101**, 147–153.

21 P. A. Fernandes, P. M. P. Salomé and A. F. da Cunha, Study of polycrystalline Cu_2ZnSnS_4 films by Raman scattering, *J. Alloys Compd.*, 2011, **509**, 7600–7606.

22 J. J. Scragg, P. J. Dale, D. Colombara and L. M. Peter, Thermodynamic Aspects of the Synthesis of Thin-Film Materials for Solar Cells, *ChemPhysChem*, 2012, **13**, 3035–3046.